



Control of valence and conduction band energies in layered transition metal phosphates via organic functionalization

Journal:	<i>Physical Chemistry Chemical Physics</i>
Manuscript ID	CP-ART-02-2016-000994.R1
Article Type:	Paper
Date Submitted by the Author:	20-Apr-2016
Complete List of Authors:	Lentz, Levi; Massachusetts Institute of Technology, Mechanical Engineering Kolb, Brian; Massachusetts Institute of Technology, Mechanical Engineering Kolpak, Alexie; Massachusetts Institute of Technology, Mechanical Engineering

SCHOLARONE™
Manuscripts



Physical Chemistry Chemical Physics

ARTICLE

Control of valence and conduction band energies in layered transition metal phosphates via surface functionalization

Levi C. Lentz,^a Brian Kolb^a, and Alexie M. Kolpak^aReceived 00th January 20xx,
Accepted 00th January 20xx

DOI: 10.1039/x0xx00000x

www.rsc.org/

Layered transition metal phosphates and phosphites (TMPs) are a class of materials composed of layers of 2D sheets bound together via van der Waals interactions and/or hydrogen bonds. Explored primarily for use in proton transfer, their unique chemical tunability also makes TMPs of interest for forming large-scale hybrid materials. Further, unlike many layered materials, TMPs can readily be solution exfoliated to form single 2D sheets or bilayers, making them exciting candidates for a variety of applications. However, the electronic properties of TMPs have largely been unstudied to date. In this work, we use first-principles computations to investigate the atomic and electronic structure of TMPs with a variety of stoichiometries. We demonstrate that there exists a strong linear relationship between the band gap and the ionic radius of the transition metal cation in these materials, and show that this relationship, which opens opportunities for engineering new compositions with a wide range of band gaps, arises from constraints imposed by the phosphorus-oxygen bond geometry. In addition, we find that the energies of the valence and conduction band edges can be systematically tuned over a range of ~3 eV via modification of the functional group extending from the phosphorus. Based on the Hammett constant of this functional group, we identify a simple, predictive relationship for the ionization potential and electron affinity of layered TMPs. Our results thus provide guidelines for systematic design of TMP-derived functional materials, which may enable new approaches for optimizing charge transfer in electronics, photovoltaics, electrocatalysts, and other applications.

Introduction

The unique and tunable physics present in many 2D materials such as graphene and MoS₂ have driven increasing interest in the study and application of 2D and layered materials. Related materials such as hybrid metal organic frameworks have enabled the creation of modular functional materials that can be designed and manufactured to address the increasingly complex technological challenges of modern society¹. Transition metal phosphates (TMPs) are a class of layered materials comprised of 2D sheets bound via van der Waals interactions and/or hydrogen-bonds between out-of-plane surface functional groups^{2,3}. There has been significant interest in layered phosphates over the past several decades, particularly for applications in proton and cation transfer and gas storage⁴. More recently, phosphates have also become of interest as solid-state electrolytes for batteries^{5,6}.

In the past few years, interest in TMPs has resurged as new approaches for efficient solution exfoliation of monolayer and bilayer 2D sheets have been developed². In addition to these

capabilities, which are not currently available for graphene and other 2D materials⁷, TMPs have promise as templates for complex nanostructured materials, in part due to the relative ease of bulk TMP synthesis, which is generally performed via precipitation from a solution of *M*-fluoro complexes and phosphoric acid, with the rate of reaction dictating the crystallinity of the material⁸.

Experiments have also demonstrated that the –H or –OH groups extending from the surfaces of each 2D layer can, in many layered TMP compounds, be substituted with other covalently bound organic moieties to form highly ordered organic-inorganic superlattices. For example, a modification of the Zr(HPO₄)₂ structure in which the hydroxyl groups have been replaced with biphenyl to form crystalline Zr(HPO₄)(H₁₁C₁₂PO₃) has been demonstrated⁹. Other experiments have shown that such surface functionalization can be controlled over a range of layered TMPs and functional groups, suggesting that these materials may provide a powerful avenue for the design of new multifunctional materials^{2,10}.

^a Department of Mechanical Engineering, Massachusetts Institute of Technology,
77 Massachusetts Avenue, Cambridge, MA, 02139

† Footnotes relating to the title and/or authors should appear here.

Electronic Supplementary Information (ESI) available: [details of any supplementary information available should be included here]. See DOI: 10.1039/x0xx00000x

For many potential applications of TMPs, especially in battery and photovoltaic devices, understanding how the electronic structure and properties change with surface functionalization is of significant interest. To date, however, the electronic properties of TMPs have been studied primarily as intercalation compounds for battery applications. Most notably, LiFePO_4 has been shown to have promising cycling characteristics.¹¹ However, electronic properties such as bandgap and band energies for layered TMP materials have not been studied in detail. In this work, we employ *ab initio* computations to investigate the atomic and electronic structure of a variety of layered TMPs in their 2D sheet with different crystal structures, chemical compositions, and functional groups. We report key electronic structure properties, including band gap (E_g), electron affinity (EA), and ionization potential (IP), and we identify relationships between these properties and the structural and chemical properties of the materials. In particular, we demonstrate that the energy levels of the band edges (*i.e.*, EA and IP) can be systematically tuned over a range of up to 1-3 eV by changing the out-of-plane functional group bound to the in-plane phosphorus. Our work suggests new approaches for control of band alignment at hetero-interfaces, and may thus lead to improved performance in numerous applications, such as photovoltaics, photo- and electro-catalysts, batteries, and other technologies in which interfacial charge transfer plays an important role.

Computational Section

Structure optimization and electronic structure calculations were performed using the planewave DFT packages Quantum Espresso (QE)¹² and Vienna Ab-initio Suite Package (VASP)¹³⁻¹⁶ with the GGA-PBE formulation of the exchange-correlation^{17,18} and ultrasoft pseudopotentials¹⁹. All pseudopotentials were obtained from existing QE and VASP libraries and tested by computing the structural properties of the ground state elemental phase at standard temperature and pressure, as well as the structural properties of the relevant phosphates as discussed above. All calculations were performed with an energy cutoff of 820 eV and forces on all atoms were converged to < 10 meV/Å. Ionization potentials and electron affinities were determined by referencing the computed band edges of isolated 2D sheets to the vacuum energy.

Once fully relaxed structures were obtained in QE, the GW formalism was employed within VASP to accurately calculate the band gap. (We note that VASP was used for GW calculations due to a more robust GW interface, but both codes are expected to give the same results. Indeed, we find that the DFT-computed band gaps and lattice parameters of the TMPs shown in Fig. 1 differ by $< 1\%$ on average between the two codes.) For all GW calculations, a cutoff of 150 eV was used to sample G-vectors, and at least 256 bands and 96 points sampling imaginary frequency space were employed. The number of bands was converged with respect to the band gap to guarantee convergence of the band gap. The vertex correction is not treated in this work due to the size of the systems studied.²⁰ Standard VASP pseudopotentials were

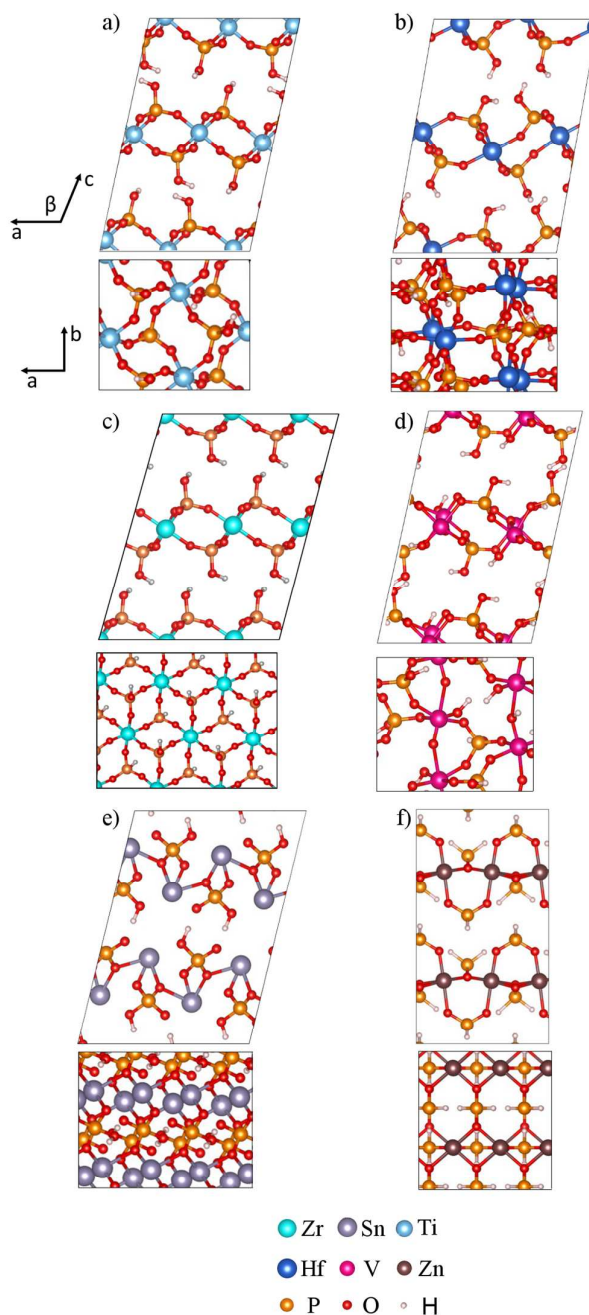


Figure 1. Atomic structures of the a-c (top) and a-b (bottom) planes of a) $\alpha\text{-Ti}(\text{HPO}_4)_2$, b) $\alpha\text{-Hf}(\text{HPO}_4)_2$, c) $\alpha\text{-Zr}(\text{HPO}_4)_2$, d) $\text{V}(\text{OH})(\text{HPO}_4)$, e) $\text{Sn}(\text{HPO}_4)$, and f) $\text{Zn}(\text{PH}_2\text{O}_2)_2$.

chosen to include the maximum number of semi-core states in the valence, and those specifically designed for GW calculations were employed when available.

Once the ground state lattice constants and atomic positions were determined, the materials were examined in their monolayer state. Only GW bandgaps are reported in the bulk state because of the inability of GW to scale with large unit cell volumes; by examining DOS, atomic positions, and DFT band gaps, there is little difference in the monolayer and bulk

Physical Chemistry Chemical Physics

Table 1. Optimized bulk lattice parameters of the studied materials.

Material	a [Å]	b [Å]	c [Å]	β [°]	Ref
α -Ti(HPO ₄) ₂	8.61 (8.61)	4.99 (4.99)	16.15 (16.15)	110.2 (110.2)	²²
α -Hf(HPO ₄) ₂	8.96 (8.97)	5.43 (5.43)	16.04 (16.10)	101.6 (101.6)	²²
α -Zr(HPO ₄) ₂	9.03 (9.15)	5.27 (5.32)	15.4 (15.29)	101.7 (103.85)	²³
V(OH)(HPO ₄)	6.34 (7.61)	7.54 (7.42)	9.27 (9.47)	93.2 (95.4)	²⁴
Sn(HPO ₄)	4.66 (4.61)	13.27 (13.60)	5.79 (5.82)	97.6 (98.8)	²⁵
Zn(PH ₂ O ₂) ₂	6.51 (6.48)	5.40 (5.37)	7.22 (7.41)	90.0 (90.0)	²⁶

All crystal structures are monoclinic except Zn(PH₂O₂)₂, which is orthorhombic. Computed values are within 3% of experimental values (given in parentheses) for all cases.

electronic structure for these materials. The interlayer interaction energies were found to be on the order of 3.7–11.2 meV/Å², about the same order as graphene (4.9 meV/Å²) and weaker than MoS₂ (~20 meV/Å²)²¹.

Results and Discussion

We investigate a range of TMPs with Ti, Zr, Hf, V, Zn, and Sn cations. The optimized unit cell parameters for each material are compared to experimental values in Table 1. The lattice parameters and atomic positions of all systems were relaxed to the ground state, as described in the Computational Section, and all structures were found to be within 3% of the experimental lattice parameters. Some error is due to the fact that the majority of these materials are experimentally characterized in the hydrated state; however, processing for most applications relies on dehydrating the structure. Thus, the computed structures do not include the hydrating water molecules. All materials studied in this work, as well as the referenced experimental studies, are shown in Table 1.

Of the materials reported in Table 1, the titanium, zirconium, and hafnium phosphates have been observed to form in similar crystal structures, with the metal cations in a nominal 4⁺ valence state. While the stacking registry of the 2D sheets varies with the metal cation, as illustrated in Figs. 1, these structures are all characterized by a 2D hexagonal sub-lattice of metal cations, with all of the cations octahedrally coordinated by oxygens from the phosphate groups. As Fig. 1 shows, the phosphate groups in these materials form tetrahedra that extend to either side of the 2D plane, with all P–OH bonds directed outward (away from the plane of metal cations). Consequently, in contrast to other 2D materials such as graphene and MoS₂, in which the 2D layers interact primarily via van der Waals interactions, neighboring 2D sheets in these phosphates are bound together by a network of hydrogen bonds (H-bonds). The H-bonding helps to preserve the interlayer stacking registry. Further, although H-bonds are stronger than van der Waals interactions, their presence enables facile exfoliation of TMP monolayers, as the interlayer H-bonds can be displaced by H-bonds formed between surface –OH groups and water molecules.

Due to the preferred 3⁺ valence state of vanadium, an analogous V(HPO₄)₂ compound has not been observed experimentally; a related compound, VO(OH)(HPO₄), has been synthesized. Although the stoichiometry is different, this material shares structural characteristics with the M(HPO₄)₂ compounds discussed above, with 6-fold coordinated vanadium cations. However, although all of the metal ligands are comprised of O atoms, the oxygens are not all from phosphate groups as in the M(HPO₄)₂ materials. Instead, as illustrated in Fig. 1d, nearest-neighbor vanadium cations are connected via a single oxygen atom, and next-nearest-neighbor vanadium cations are connected through –PO₄ groups; each V cation also has an –OH ligand. This structure leads to two inequivalent –PO₄ tetrahedra, one normal to the vanadium plane and the other tilted with respect to the vanadium plane. As a result of this geometry, bulk VO(OH)(HPO₄) exhibits a higher density of interlayer H-bonds and thus a larger interlayer binding energy compared to the M(HPO₄)₂ compounds.

A related zinc compound, Zn(H₂PO₂)₂, has been synthesized. As with most zinc compounds, zinc has a nominal 2⁺ valence state in this material. The 6-fold coordinated Zn cations are linked by –O–PH₂–O– moieties such that all of the Zn ligands are oxygens from phosphorous groups (Fig. 1f). Unlike the other structures examined in this work, there are no out-of-plane –OH groups and thus no interlayer H-bonding in this structure. Therefore, Zn(H₂PO₂)₂ has the lowest interlayer binding energy of the materials in this work.

Finally, we consider tin phosphate. Although Sn is not a transition metal, it is of particular interest as mixed-cation phosphates based on Zr(HPO₄)₂ have been synthesized²⁷. While pure Sn(HPO₄)₂ has not been synthesized to date, Sn(HPO₄), with tin in the 2⁺ state, has been successfully made. Here we consider both compounds. We find that the former exhibits an optimized structure similar to those formed by the other 4⁺ cations in this study, while the latter has been shown experimentally to form 2D sheets in which the metal cations are non-planar. The origin of this distorted geometry is the presence of the lone pair of non-bonding electrons that occupy the 5s orbitals on the Sn²⁺ cations, resulting in steric repulsion, as can be seen in Fig. 1e.

The band gap of a material is extremely important in many devices, including solar absorbers, photocatalysts,

Table 2. Bandgaps computed for studied materials.

Material	Cation Valence	r_{cat} [Å]	E_g^{DFT}	E_g^{GW}
V(OH)(HPO ₄)	3+	0.64	1.57	4.77
α -Ti(HPO ₄) ₂	4+	0.68	2.82	4.78
Sn(HPO ₄) ₂ [†]	4+	0.71	3.29	4.88
Zn(H ₂ PO ₂) ₂	2+	0.74	4.34	6.62
Zn(HPO ₄) ₂ [‡]	2+	0.74	4.14	6.81
α -Hf(HPO ₄) ₂	4+	0.78	4.81	6.7
α -Zr(HPO ₄) ₂	4+	0.79	5.04	6.92
Sn(HPO ₄)	2+	0.93	3.30	4.88

r_{cat} is Shannon ionic radius of the cation; E_g^{DFT} is the DFT bandgap and E_g^{GW} is the G₀W₀ bandgap, both in eV. Materials marked with [†] and [‡] were computed in the α -Zr(HPO₄)₂ and Sn(HPO₄) structures, respectively. The computational cost of G₀W₀ meant only experimental structures were run within G₀W₀.

electrocatalysts, and transparent conductors. By examining the literature on these materials, no experimental measurements of the band gap have been reported for any of the TMPs studied in this work. It is well known that DFT is unable to predict accurate band gaps²⁸. We therefore perform higher accuracy G₀W₀ computations, as described in the Computational Section, using the DFT-optimized structural parameters to determine accurate band gaps²⁹. Table 2 shows both the G₀W₀ and DFT band gaps for the materials that have previously been synthesized (those in Table 1). In this work we present design guidelines for high-throughput screening. While it is important to note the accurate band gap through GW calculations, trends presented are of interest in DFT-space due to the combination of relatively cheap cost of the calculations combined with the accuracy of predicting trends in material properties.

Figure 2 shows that the magnitude of the band gap increases with increasing ionic radius of the metal cation. This relationship arises from differences in the chemical environments represented by the differences in stoichiometries in the systems. The wide range of materials studied make it difficult to determine the exact cause of this relationship to be described with certitude, however a combination of orbital overlap and NN metal ions seem to be driving this trend. With the exception of Sn(HPO₄), discussed further below, the correlation between cation radius and band gap is described very well with a linear fit, as illustrated in the figure, providing a strong, predictive structure-property relationship to guide further design.

In contrast to the other materials in this work, Sn(HPO₄) exhibits a non-planar cation arrangement, which arises from steric effects due to the lone pair of electrons on Sn²⁺. The resulting distorted geometry explains why the relationship between band gap and cation radius does not apply for this material. This is confirmed by computing the band gap of Sn(HPO₄)₂, in which the Sn is in the 4⁺ valence state and thus no longer has a lone pair of 5s electrons. As Table 2 shows, this material follows the general trend. Substituting Sn for Zn in

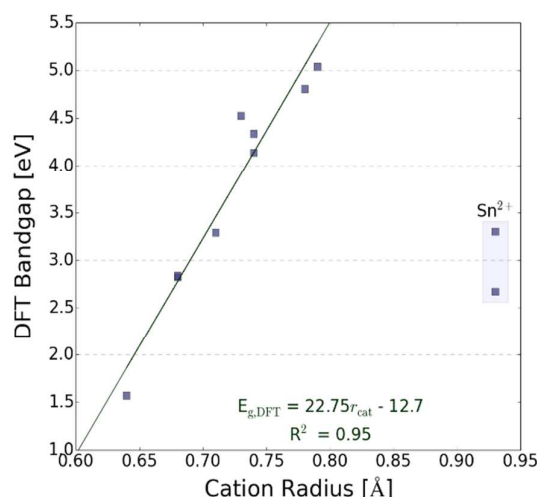


Figure 2 DFT band gap versus Shannon ionic radius of the metal cation. The outlier points from the Sn²⁺ structures are not included in the fit (see text). The DFT trend is of particular interest because of the high-throughput design principles of DFT, allowing for speedy material selection.

Zn(H₂PO₂)₂ provides further evidence for this effect, as the presence of Sn²⁺ in this compound also leads to a distorted structure with a band gap does not follow the trend; this material is the other outlier in Fig. 2. In contrast, substituting Zn into Sn(HPO₄) gives a band gap approximately the same as that of Zn(H₂PO₂)₂, as shown in Table 2. These results further confirm the generality of the relationship between cation radius and band gap. Furthermore, they suggest that substitution of Group 14 cations in the 2+ valence state may be a useful approach for engineering the band gap.

The large band gaps of the layered TMPs make them non-ideal for application as active materials in photovoltaic devices. However, applications such as transparent conductors can be imagined. The ability to easily exfoliate thin TMP films might enable efficient and inexpensive top-layer growth in applications for which transparent conducting oxides are currently employed. Further, as shown below, functional modification of the surface enables one to achieve a wide range in the energies of the conduction and valence band levels, potentially enabling a new route for design of materials for a range of applications in which precise control of band alignment is critical.

Figure 3a shows that substitution of different functional groups for the surface -OH (namely -H, -NH₂, -CH₃, and -F, which can be visualized in Figure 5) enables large variations in the energies of the band edges, i.e., the ionization potential and electron affinity of the base material. The figure also shows that this phenomenon can be well described as a linear relationship between the energies of the conduction and valence band edges and the Hammett constant, σ_p , of the functional group. This constant is a measure of the electron donating or electron withdrawing character of a functional group. Initially derived from relationships observed upon substitution of hydrogen on benzene with various functional groups, σ_p has subsequently been used to describe the behaviour in many other organic systems³⁰. As Fig. 3a shows, the relationship between σ_p and the band edges for the

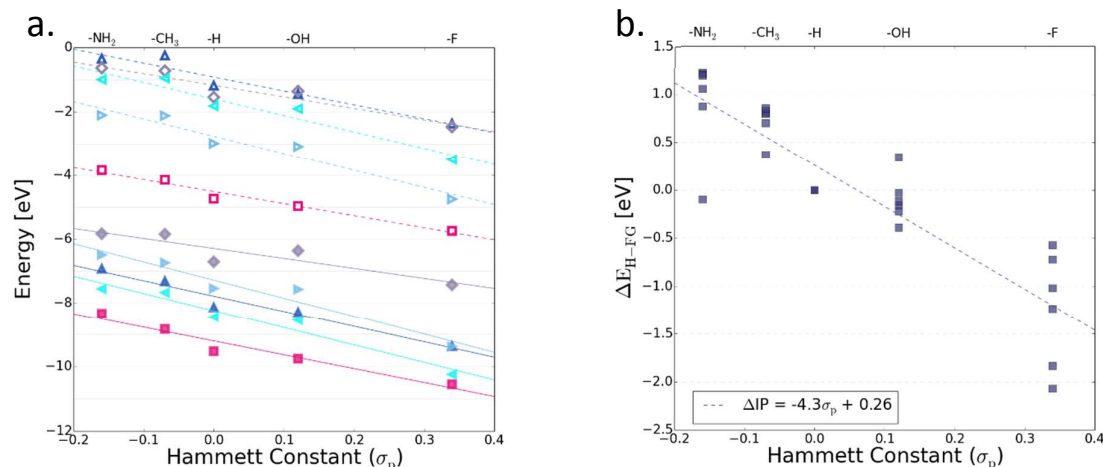


Figure 3. a) Energy variation of the valence and conduction band edges with substitution of surface group R , represented by the Hammett constant of R (bottom) and chemical formula (top). Band edges are referenced to the vacuum level (shown as zero on the graph), giving the magnitude of the IP and EA. Upwards triangles are α -Hf(RPO₃)₂ (dark blue); diamonds are Sn(RPO₃) (grey); right triangles are α -Ti(RPO₃)₂ (light blue); squares are V(OH)(RPO₃) (pink); and left triangles are α -Zr(RPO₃)₂ (cyan). Solid and dashed lines are fits for the EA and IP, respectively. b) By taking the energetic difference between the $-H$ group and other functional groups for the IP, a single linear trend to reasonably describe the relationship between IP and σ_p for all of the studied materials. The dashed line is the least squared best fit line.

layered TMPs is strongly linear, with $R^2 > 0.80$ for all materials except for Zn(H₂PO₂)₂ which has $R^2 = 0.6$; this deviation is likely due to the fact that none of the $-PO_4$ tetrahedra are normal to the transition metal plane in Zn(H₂PO₂)₂. All $M(HPO_4)_2$ show very good fits, with $R^2 > 0.92$.

Further, we find that shifting the valence band edges (*i.e.*, the IP) so that the value for $R = -OH$ is set to zero for all materials and then fitting all of the data gives the following general In addition, we note that, due to the 2D nature of the TMPs, functionalization leads to bulk electronic structures changes, in contrast to surface functionalization of typical crystalline semiconductors which causes band bending at the surface, but

relationship: $IP \approx -4.30\sigma_p + 0.26 + IP_{ref}$ [eV], where IP_{ref} is the ionization potential of a reference material with an $-OH$ functional group. As shown in Fig. 3b, this fit gives a reasonable R^2 value of 0.79, showing that our results enable semi-quantitative prediction of the IP and EA for a wide range of 2D TMPs as a function of R group, based on only a single measurement or calculation of the valence band edge of a reference material.

leaves the bulk electronic structure unchanged. This effect could be very important in terms of charge transfer at interfaces, as band bending may lead to undesired energy barriers and depletion regions.

Figure 4 shows that the energetic shift is essentially the same for the VBE and CBE for a given TMP. Therefore, functionalization enables one to shift the energies of the band edges without changing the band gap. Among other uses, this capability could enable tuning of band alignment in, *e.g.*, photovoltaic devices, without changing the optical properties of the material, thereby addressing a common problem in designing transparent conducting contacts.

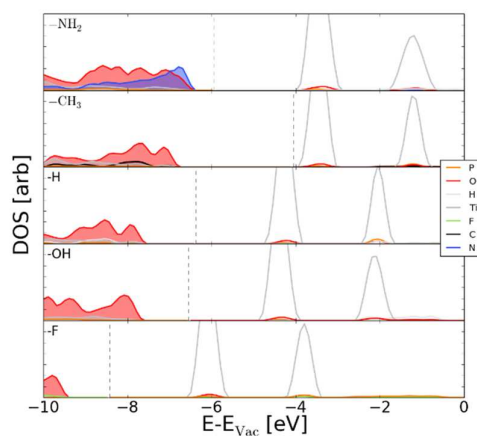


Figure 4. Projected density of states for a monolayer of α -Ti(RPO₃)₂ with various functional groups. Shaded and unshaded curves are occupied and unoccupied states, respectively. Vertical dashed lines indicate the position of the Fermi level. Note that the energy is referenced to the vacuum level to illustrate the change in the position of the valence band edge with different R .

We further investigate the origin of the relationship between the functional group and the IP and EA of the TMPs by examining the computed projected density of states (pDOS) and the 3D charge densities of states at the CBM and VBM. As an example, Figure 4 shows the pDOS and charge density isosurfaces of α -Ti(RPO_3)₂ with $R = -NH_3, -CH_3, -H, -OH, -F$. The functionalization has a larger effect on the valence band because it is composed primarily of O p -states that can hybridize with states in the functional group, while the CBM is composed primarily of metal d -states with the contributing oxygen states coming from the oxygen in the M -O-P bonds. Substitution of the out-of-plane $-OH$ group does not affect these states. All materials closely follow this trend, especially the $M(HPO_4)_2$ structures. Again, we emphasize that, even with these changes, the magnitude of the band gap remains constant within each base material.

Figure 5 shows the charge density of states at the CBM and VBM of titanium phosphate with each of the functional groups indicated in Figure 4. These figures illustrate that states due to the functional group substitution are highly localized with little hybridization. The $-NH_2$ group is an outlier in this case because it leads to a distorted structure, as illustrated in Figure 5, in which the orientation of the functional group causes increased orbital overlap at the interface, leading to the additional states at the valence band edge. This is due to the hydrogen bonding present in $-NH_2$ groups; out of plane reconstructions like this do not change the overall trend observed.

Except in the case of $-NH_2$, substitution of the $-OH$ in the phosphates generally does not lead to either the formation of dangling bonds or new states involving other atoms on the lattice, because the P atom to which they bind is geometrically isolated and has localized states. This minimizes reconstruction at the surface, enabling a wide range of functional groups to modify the EA and IA with little effect on the interactions of the in-plane lattice. The shift in the band edges relative to the vacuum can thus be explained as arising from charge redistribution between the 2D sheet and the substituted functional group.

Conclusions

In this work, we computed the atomic and electronic structure of a set of 2D TMPs spanning a large range of compositions. We show that the band gap of these materials can be systematically tuned by changing the ionic radius of the metal cation within a variety of different phosphate and phosphite compounds, and we suggest that stabilization of 2^+ cations from the Group 14 metals as a promising approach for breaking the observed trend and achieving materials with smaller band gaps. Furthermore, we show that, through simple functionalization of the TMP layers, the ionization potential and electron affinity of a base TMP can be systematically tuned over a wide range of 1-3 eV without changing the band gap.

The trends in band gap, IP, and EA with respect to fundamental properties that are identified in this work have the potential to provide useful guidelines for the design of

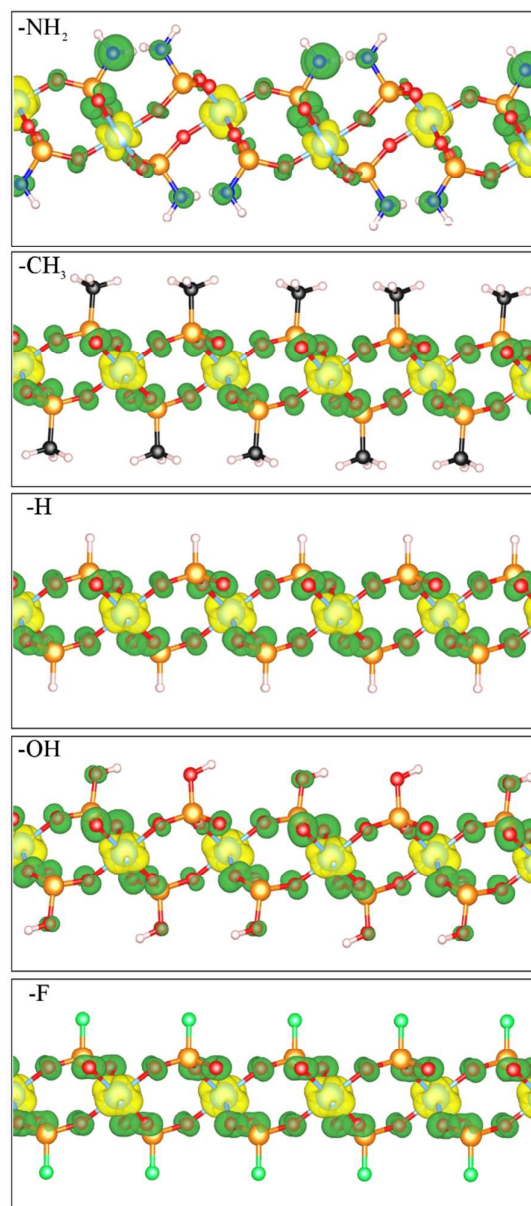


Figure 5 Isosurfaces of $\sum_k |\Psi_{r,k}|^2$, where k runs over the Brillouin zone and r corresponds to the valence (green) or conduction (yellow) band edge of α -Ti(RPO_3)₂. The only R group that significantly changes the character of the band edges is $-NH_2$.

materials for a variety of applications. For example, this could enable rational design of charge blocking layers that exhibit ideal band alignment with specified absorbers and thereby optimize the open-circuit voltage of photovoltaic devices without compromising transparency; catalytic surface coatings with band edges at ideal energies for a variety of electrocatalytic reactions; and heterostructures with optimized band alignment for many other applications. Further, the ability to systematically tune the band edges of these materials via organic functionalization, combined with the ease of monolayer and bilayer exfoliation and the existence of numerous layered TMPs with similar structures, provides

exciting opportunities for the design of novel TMP superlattices with a variety of novel functionalities.

Acknowledgements

L. C. L. acknowledges support from the S3TEC EFRC. B. K. acknowledges support from the CNGMD EFRC.

Notes and references

‡ Footnotes relating to the main text should appear here. These might include comments relevant to but not central to the matter under discussion, limited experimental and spectral data, and crystallographic data.

§

§§

etc.

- (1) Butler, S. Z.; Hollen, S. M.; Cao, L.; Cui, Y.; Gupta, J. A.; Gutiérrez, H. R.; Heinz, T. F.; Hong, S. S.; Huang, J.; Ismach, A. F.; Johnston-Halperin, E.; Kuno, M.; Plashnitsa, V. V.; Robinson, R. D.; Ruoff, R. S.; Salahuddin, S.; Shan, J.; Shi, L.; Spencer, M. G.; Terrones, M.; Windl, W.; Goldberger, J. E. Progress, Challenges, and Opportunities in Two-Dimensional Materials Beyond Graphene. *ACS Nano* **2013**, *7* (4), 2898–2926.
- (2) *Metal Phosphonate Chemistry*; Clearfield, A., Demadis, K., Eds.; Royal Society of Chemistry: Cambridge, 2011.
- (3) Vivani, R.; Alberti, G.; Costantino, F.; Nocchetti, M. New Advances in Zirconium Phosphate and Phosphonate Chemistry: Structural Archetypes. *Microporous Mesoporous Mater.* **2008**, *107* (1–2), 58–70.
- (4) Díaz, A.; Mosby, B. M.; Bakhmutov, V. I.; Martí, A. A.; Batteas, J. D.; Clearfield, A. Self-Assembled Monolayers Based Upon a Zirconium Phosphate Platform. *Chem. Mater.* **2013**, *25* (5), 723–728.
- (5) Saubanère, M.; Yahia, M. B.; Lebègue, S.; Doublet, M.-L. An Intuitive and Efficient Method for Cell Voltage Prediction of Lithium and Sodium-Ion Batteries. *Nat. Commun.* **2014**, *5*.
- (6) Adams, S.; Rao, R. P. High Power Lithium Ion Battery Materials by Computational Design. *Phys. Status Solidi A* **2011**, *208* (8), 1746–1753.
- (7) Cai, M.; Thorpe, D.; Adamson, D. H.; Schniepp, H. C. Methods of Graphite Exfoliation. *J. Mater. Chem.* **2012**, *22* (48), 24992–25002.
- (8) Alberti, G.; Casciola, M.; Costantino, U.; Vivani, R. Layered and Pillared metal(IV) Phosphates and Phosphonates. *Adv. Mater.* **1996**, *8* (4), 291–303.
- (9) Clearfield, A.; Wang, Z. Organically Pillared Microporous Zirconium Phosphonates. *J. Chem. Soc. Dalton Trans.* **2002**, No. 15, 2937–2947.
- (10) Sadaoka, Y.; Matsuguchi, M.; Sakai, Y.; Mitsui, S. Electrical Properties of α -Zirconium Phosphate and Its Alkali Salts in a Humid Atmosphere. *J. Mater. Sci.* **1988**, *23* (8), 2666–2675.
- (11) Yuan, L.-X.; Wang, Z.-H.; Zhang, W.-X.; Hu, X.-L.; Chen, J.-T.; Huang, Y.-H.; Goodenough, J. B. Development and Challenges of LiFePO₄ Cathode Material for Lithium-Ion Batteries. *Energy Environ. Sci.* **2011**, *4* (2), 269–284.
- (12) Giannozzi, P.; Baroni, S.; Bonini, N.; Calandra, M.; Car, R.; Cavazzoni, C.; Ceresoli, D.; Chiarotti, G. L.; Cococcioni, M.; Dabo, I.; Corso, A. D.; Gironcoli, S. de; Fabris, S.; Fratesi, G.; Gebauer, R.; Gerstmann, U.; Gougoussis, C.; Kokalj, A.; Lazzeri, M.; Martin-Samos, L.; Marzari, N.; Mauri, F.; Mazzarello, R.; Paolini, S.; Pasquarello, A.; Paulatto, L.; Sbraccia, C.; Scandolo, S.; Sclauzero, G.; Seitsonen, A. P.; Smogunov, A.; Umari, P.; Wentzcovitch, R. M. QUANTUM ESPRESSO: A Modular and Open-Source Software Project for Quantum Simulations of Materials. *J. Phys. Condens. Matter* **2009**, *21* (39), 395502 (19pp).
- (13) Kresse, G.; Hafner, J. Ab Initio Molecular Dynamics for Liquid Metals. *Phys. Rev. B* **1993**, *47* (1), 558.
- (14) Kresse, G.; Hafner, J. Ab Initio Molecular-Dynamics Simulation of the Liquid-Metal–amorphous-Semiconductor Transition in Germanium. *Phys. Rev. B* **1994**, *49* (20), 14251.
- (15) Kresse, G.; Furthmüller, J. Efficiency of Ab-Initio Total Energy Calculations for Metals and Semiconductors Using a Plane-Wave Basis Set. *Comput. Mater. Sci.* **1996**, *6* (1), 15–50.
- (16) Kresse, G.; Furthmüller, J. Efficient Iterative Schemes for Ab Initio Total-Energy Calculations Using a Plane-Wave Basis Set. *Phys. Rev. B* **1996**, *54* (16), 11169.
- (17) Perdew, J. P.; Burke, K.; Ernzerhof, M. Generalized Gradient Approximation Made Simple. *Phys. Rev. Lett.* **1996**, *77* (18), 3865–3868.
- (18) Perdew, J. P.; Chevary, J. A.; Vosko, S. H.; Jackson, K. A.; Pederson, M. R.; Singh, D. J.; Fiolhais, C. Atoms, Molecules, Solids, and Surfaces: Applications of the Generalized

- Gradient Approximation for Exchange and Correlation. *Phys. Rev. B* **1992**, *46* (11), 6671–6687.
- (19) Vanderbilt, D. Soft Self-Consistent Pseudopotentials in a Generalized Eigenvalue Formalism. *Phys. Rev. B* **1990**, *41* (11), 7892–7895.
- (20) Romaniello, P.; Guyot, S.; Reining, L. The Self-Energy beyond GW: Local and Nonlocal Vertex Corrections. *J. Chem. Phys.* **2009**, *131* (15), 154111.
- (21) Rydberg, H.; Dion, M.; Jacobson, N.; Schröder, E.; Hyldgaard, P.; Simak, S. I.; Langreth, D. C.; Lundqvist, B. I. Van Der Waals Density Functional for Layered Structures. *Phys. Rev. Lett.* **2003**, *91* (12), 126402.
- (22) Salvadó, M. A.; Pertierra, P.; García-Granda, S.; García, J. R.; Rodríguez, J.; Fernández-Díaz, M. T. Neutron Powder Diffraction Study of α -Ti(HPO₄)₂·H₂O and α -Hf(HPO₄)₂·H₂O; H-Atom Positions. *Acta Crystallogr. Sect. B* **1996**, *52* (5), 896–898.
- (23) Alberti, G.; Costantino, U.; Millini, R.; Perego, G.; Vivani, R. Preparation, Characterization, and Structure of α -Zirconium Hydrogen Phosphate Hemihydrate. *J. Solid State Chem.* **1994**, *113* (2), 289–295.
- (24) Le Bail, A.; Ferey, G.; Amoros, P.; Beltran-Porter, D. Structure of Vanadyl Hydrogenphosphate Dihydrate α -VO(HPO₄)·2H₂O Solved from X-Ray and Neutron Powder Diffraction. *Eur. J. Solid State Inorg. Chem.* **1989**, *26* (4), 419–426.
- (25) Schroeder, L.; Prince, E. Hydrogen-Bonded Dimers in Tin (II) Hydrogen Phosphate. *Acta Crystallogr. B* **1976**, *32* (12), 3309–3311.
- (26) Tanner, P. A.; Yu-Long, L.; Mak, T. C. Synthesis, Crystal Structures and Vibrational Spectra of Zinc Hypophosphites. *Polyhedron* **1997**, *16* (3), 495–505.
- (27) Valsaraj, P. V.; Janardanan, C. Comparative Studies on Proton Conducting Nature of Copper Selective Tin Zirconium Phosphate Cation Exchanger with Its Single Salts Counter Parts. *Res. J. Chem. Sci. ISSN 2231*, 606X.
- (28) Hybertsen, M. S.; Louie, S. G. First-Principles Theory of Quasiparticles: Calculation of Band Gaps in Semiconductors and Insulators. *Phys. Rev. Lett.* **1985**, *55* (13), 1418–1421.
- (29) Aryasetiawan, F.; Gunnarsson, O. The GW Method. *Rep. Prog. Phys.* **1998**, *61* (3), 237.
- (30) Hansch, C.; Leo, A.; Taft, R. W. A Survey of Hammett Substituent Constants and Resonance and Field Parameters. *Chem. Rev.* **1991**, *91* (2), 165–195.